

Document downloaded from:

<http://hdl.handle.net/10251/121822>

This paper must be cited as:

Urbaniak, A.; Pawlowski, M.; Marzantowicz, M.; Marí, B.; Sall, T. (2018). Study of the effect of V-doping on the opto-electrical properties of spray-pyrolized SnS thin films. *Thin Solid Films*. 664:60-65. <https://doi.org/10.1016/j.tsf.2018.08.032>



The final publication is available at

<http://doi.org/10.1016/j.tsf.2018.08.032>

Copyright Elsevier

Additional Information

Accepted Manuscript

Study of the effect of V-doping on the opto-electrical properties of spray-pyrolized SnS thin films

A. Urbaniak, M. Pawłowski, M. Marzantowicz, B. Marí, T. Sall



PII: S0040-6090(18)30563-7
DOI: [doi:10.1016/j.tsf.2018.08.032](https://doi.org/10.1016/j.tsf.2018.08.032)
Reference: TSF 36842
To appear in: *Thin Solid Films*
Received date: 4 April 2018
Revised date: 22 August 2018
Accepted date: 22 August 2018

Please cite this article as: A. Urbaniak, M. Pawłowski, M. Marzantowicz, B. Marí, T. Sall, Study of the effect of V-doping on the opto-electrical properties of spray-pyrolized SnS thin films. *Tsf* (2018), doi:[10.1016/j.tsf.2018.08.032](https://doi.org/10.1016/j.tsf.2018.08.032)

This is a PDF file of an unedited manuscript that has been accepted for publication. As a service to our customers we are providing this early version of the manuscript. The manuscript will undergo copyediting, typesetting, and review of the resulting proof before it is published in its final form. Please note that during the production process errors may be discovered which could affect the content, and all legal disclaimers that apply to the journal pertain.

Study of the effect of V-doping on the opto-electrical properties of spray-pyrolized SnS thin films

A. Urbaniak^{1*}, M. Pawłowski¹, M. Marzantowicz¹, B. Mari², T. Sall²

¹Faculty of Physics, Warsaw University of Technology, Koszykowa 75, PL 00 662 Warszawa, Poland

²Insitut de Disseny i Fabricació, Universitat Politècnica de València, Cami de Vera s/n, 46022 Valencia, Spain

ACCEPTED MANUSCRIPT

Abstract

SnS is an earth-abundant material that is a potentially suitable candidate for the absorber layer in solar cells. Here spray-pyrolized SnS thin films doped with vanadium were studied using structural and opto-electrical methods. The thin films have an orthorhombic structure with a preferential (111) crystallographic direction. SnS has an indirect bandgap of around 1.05 eV, whereas doping with vanadium changes the band edge and shifts the absorption threshold to around 1.2 eV. The photoluminescence study revealed a broad peak related to the band-to-band transition of energy at around 1.2 eV and an additional sharp peak positioned at 1.17 eV related to vanadium. Additionally, a non-radiative recombination mechanism followed by hopping through band fluctuation barriers has been proposed for photoluminescence quenching at increased temperatures. The conductivity measurements reveal that conductivity weakly increases with V-doping, whereas its activation energy decreases from around 0.38 eV to 0.35 eV.

Keywords: Tin sulfide; Thin films; Photovoltaics; Spray pyrolysis; Photoluminescence

Introduction

The efficiency of conventional solar cells is related to the balance between the generation and recombination of photo-induced electron-hole pairs. Additionally, if the photon energy is greater than the semiconductor energy bandgap needed to generate an electron-hole pair, this excess energy is lost due to the rapid thermalization to the band extremum. The limit of photovoltaic conversion efficiency for a single bandgap solar cell was calculated by Shockley and Queisser [1] (the so called S-Q limit) using a detailed balance theory. For the AM1.5 sun spectrum, the limit places the maximum efficiency at around 33.7% for a bandgap of 1.34 eV [2]. Several concepts have been presented to overcome the S-Q limit. One approach is to increase the photocurrent by a two-step excitation that employs an isolated intermediate band (IB) located within the bandgap of the host material. By inserting this additional band into the forbidden bandgap, two additional transitions (VB-IB and IB-CB) are allowed at energies lower than the bandgap energy, therefore enabling the absorption of subbandgap photons (Figure 1).

The theoretical limit for the efficiency of a single-junction solar cell with IB is 63.2% for a semiconductor with a bandgap of 1.98 eV [3]. The beneficial effect of an IB on photocurrent generation occurs for the absorbers with bandgap energies greater than 1.14 eV [4]. However, there are additional features that an intermediate band should have. It should be delocalized and indiscrete to minimize the non-radiative recombination. Additionally, it should not overlap with the valence or conduction bands to prevent the thermalization of charge carriers to the IB. Finally, the IB should be partially occupied by electrons to increase the probability of the lower energy transition (E_2 in Figure 1). Even though many materials have been proposed and investigated, to our knowledge, the semiconductor and its dopant that fulfill all the requirements for the perfect material with an intermediate band have yet to be found. However, one of the promising pathways consists of doping semiconductors with transition metals. Depending on the crystal symmetry, transition metals can introduce their d orbitals within the bandgap of a host material [5], thus allowing the formation of the isolated band when their concentration is at the atomic level. Theoretical studies utilizing density functional theory (DFT) have proposed many host-dopant pairs for the photovoltaic absorbers to form an intermediate band. They include GaAs:Ti [6], Si:Au [7], Si:Ti [8], CuGaSe₂:Cr [9], CdTe:Sn [10], In₂S₃:V [11], and SnS₂:(V,W) [12]. However, the last two materials are more likely to be used as the buffer or window layer of a solar cell due to their wide bandgaps. Here we focus our attention on SnS, which is considered a solar cell absorber. Even though it has an indirect bandgap of around 1.1 eV its absorption is dominated by direct transitions with energies around 1.4–1.5 eV [13]. This large offset between its effective absorption and the bandgap is undesirable because the energy difference is lost due to thermalization. However, introducing an intermediate band to the material could enable the additional absorption of low energy photons and lower the losses due to thermalization. Here we prepared V-doped SnS thin films by spray pyrolysis [14][15] and studied their basic electrical and optical properties.

Experimental

Thin film preparation

The SnS thin films were prepared by chemical spray pyrolysis from an aqueous solution containing tin (II) chloride dihydrate ($\text{SnCl}_2 \cdot 2\text{H}_2\text{O}$), thiourea ($\text{CS}(\text{NH}_2)_2$), and vanadium chloride (VCl_4) at different percentages (0%, 2%, 4%, and 6%). The surface tension of water was reduced by adding 10% ethanol to the solution. The molarities of both solutes were 0.1 M. Due to the dissolution of $\text{SnCl}_2 \cdot 2\text{H}_2\text{O}$ in bi-distilled water, the stannous chloride dihydrate was dissolved with 37% chloride acid before adding it to the sulfur solution. The solution was sprayed at a rate of 1.5 mL min^{-1} on a heated soda-lime glass substrate for 4 min, which was kept in an ultrasonic bath and cleaned with acetone, distilled water, and ethanol prior to use. The substrate temperature was kept constant at 350°C . The compressed air was used as a carrier gas and its pressure was 700 hPa, and the distance from the nozzle to the substrate was 25 cm. To avoid growth of the Sn_2S_3 and SnS_2 phases, Sn(II) was used instead of Sn(IV) [16]. The SnS thin films were grown using the technique described in Sall et al.[17][18]. Based on the previous studies [18] we have estimated the $[\text{Sn}]/[\text{S}]$ ratio to be close to one.

Thin film characterization

The structural properties of the prepared SnS:V thin films were verified by X-Ray Diffraction (XRD) using a Rigaku Ultima IV diffractometer with the Bragg-Brentano configuration and $\text{Cu:K}\alpha$ radiation ($\lambda = 15.418 \text{ nm}$). The data were collected in the 10° – 60° 2θ range, with a step size of 0.02° . The morphology of the film surface was analyzed using an NT-MDT NTEGRA PRIMA atomic force microscope in semi-contact mode. The optical characterization, including the transmittance and reflectance measurements, was carried out using the Bentham PVE300 setup in the 300–1800 nm light wavelength range. The setup was equipped with halogen and wolfram lamps and Ge and Si photodetectors. The reflectance was measured using an integration sphere that collected the diffused light. For the photoluminescence (PL) measurements, the 514.5 nm line of an Ar^+ laser was used for the excitation in the 4–500 mW power output range, which corresponds to the light power density range of approximately 100 mW cm^{-2} to 12.5 W cm^{-2} . The lock-in technique was used for the excitation, where the signal was collected with an iHR550 grating monochromator and then detected by a nitrogen-cooled Ge detector. The samples were cooled in a helium closed-cycle setup, and the PL spectra were analyzed in the 10–100 K temperature range. Al electrodes were evaporated on the SnS films in a planar configuration to perform the electrical measurements. The electrodes were in the form of stripes, around 300 nm thick and the distance between electrodes was 4 mm. The conductivity was measured in a liquid nitrogen-cooled cryostat in the 80–330 K temperature range.

Results and discussion

Structural analysis

The diffraction spectra of the synthesized SnS:V thin films are presented in Figure 1. All of the synthesized films are polycrystalline. The main diffraction peak is located at $2\theta = 31.645 \pm 0.021^\circ$, which corresponds to the (111) crystallographic direction of the SnS orthorhombic phase (JCPDS #39-0354). The peaks are broad, which is a characteristic of disordered materials and points to the small size of the crystallites. The crystallite size can be calculated by fitting the diffraction peaks with the Gaussian function defined in Scherer's equation, $\tau = k\lambda/\beta \cos \theta$, where τ is the crystallite size, k is the factor related to the crystallite shape β is the full width at half maximum of the maximum intensity peak (FWHM), and θ is the Bragg diffraction angle. In general, the k factor is defined as the ratio of FWHM to the integral breadth of the peak, which is the ratio of the peak area and its maximum height. Using this approach, we have calculated the crystallite size of investigated thin films. The crystallite size slightly increase with the V content from 19.0 Å to 20.4 Å but the change is almost within the uncertainty range. Moreover if we compare the raw XRD (111) peaks for all the samples they almost coincide. The calculated sizes are presented in Table 1.

Figure 2 shows the atomic force microscopy (AFM) images of undoped SnS and SnS:V 6% thin films. The rest of the SnS:V thin films share the features of those presented in Figure 2. The scan area was $5 \mu\text{m} \times 5 \mu\text{m}$ with a resolution of 512×512 points. The images show irregular film structures, with needle-like, longitudinal-type grains already observed in the SnS thin films prepared by spray pyrolysis [17][19]. Taking into account the error bars, as well as the shape of the grains, the mean grain size is comparable among the samples, but the roughness of the film surface increases significantly in the V-doped thin films. The calculated crystallite sizes are roughly two times smaller than the mean grain size. However, this may arise from the different parameters calculated by the XRD and AFM analyses. XRD provides the minimum crystallite size, whereas AFM images the mean size of the grain. As the grains are longitudinal, the width of the grains might actually correspond to the minimum crystallite size, as well as lower the mean grain size comparing to its length. Thus, despite the discrepancy in the XRD and AFM results, the grains might actually consist of a single crystallite.

Transmission and absorption

To obtain information on the optical properties of the investigated thin films, transmission and reflection were measured as a function of photon energy. Based on the results, the absorption coefficient (α) was calculated assuming a 1- μm thickness for the layers. The results of the calculated absorption coefficients and transmittances are presented in Figure 4. The absorption is highest in the undoped SnS thin film and for the energies above the bandgap absorption coefficient, reaching maximum values of around $8 \times 10^4 \text{ cm}^{-1}$ (Figure 4a). The V-doped SnS thin films have lower maximum absorption values, as low as around $4 \times 10^4 \text{ cm}^{-1}$, but no systematic dependence on the amount of vanadium has been observed. However, the point where the absorption saturates shifts to lower energies

in the V-doped thin films, ranging from around 2.1 eV in the undoped SnS sample to around 1.8 eV in the SnS sample doped with 6% vanadium.

Extrapolation of the straight part of $(\alpha hv)^{1/2}$ and $(\alpha hv)^2$ versus hv provides the bandgap energy of the material for indirect and direct bandgaps, respectively. The undoped SnS thin film has an indirect bandgap energy slightly below 1.1 eV (Figure 4a), which agrees well with the theoretically calculated value of 1.07 eV [13]. The band edge in the V-doped thin films does not have a clear direct or indirect character, and the absorption coefficient is not linear versus hv . The estimated energy threshold for the absorption is around 1.2 eV for all the SnS:V thin films (Figure 4a). Even though the direct transition agrees with the theoretical value of E_g , the absorption edge is wide and extends to higher energies than expected for SnS. Partially this might be caused by band tails present in highly distorted material. The second reason might be related to the formation of SnO or SnS_{1-x}O_x during the deposition in the air atmosphere. Different studies indicate different bandgap energies of SnO (i.e. 2.7 eV and 3.4 eV depending on the annealing atmosphere [20]). In one of the previous studies [18] the correlation of SnS measured band edge and oxygen content was proposed and the shift of the band edge to higher energies was interpreted as the influence of SnS_{1-x}O_x formation.

Photoluminescence

Radiative recombination processes in semiconductors can be studied by PL, which provides information about the types of radiative recombination and the defect parameters taking part in the recombination. Figure 5 shows the PL spectra for all the SnS:V thin films measured at 9.6 K. All the spectra are centered on 1.2 eV, being non-symmetrical with a more distributed low-energy part of the peak. The thin films doped with vanadium, in comparison to the undoped sample, exhibit an additional very sharp peak at 1.17 eV. The SnS bandgap energy changes with temperature. Parentau and Carlone [21] measured the energy of direct and indirect transitions in SnS at different temperatures, where they calculated the temperature coefficients dE/dT , obtaining $dE/dT = -0.36 \text{ meV K}^{-1}$ for the indirect transition. In the case of our measurements, the difference between the transmission and PL measurements is around 287 K, yielding a change in energy of the indirect bandgap of 103 meV. Therefore, we tentatively assign the 1.2 eV PL peak as the band-to-band transition, because its energy equals the indirect bandgap energy corrected for temperature. An exponential fit to the low-energy slope of the peak gives the Urbach energy E_U [22], which is related to the width of the band tails (Table 2). The 1.17 eV peak, present in the V-doped samples, is very sharp compared to the main PL signal. This PL response arises from the transitions between atomic orbitals [23] or from band transitions in high-quality crystals [24], where the energies of the electron levels are well defined in both cases. Our investigated thin films have a very low crystal quality, and it is known that the atomic orbital of some of the transition metals can locate within the bandgap of the host material [5]. Therefore, we suggest that the observed peak might be related to PL from the electron orbitals in vanadium.

We investigated the PL evolution with laser power and temperature to gain more insight into the nature of the observed PL signal. The results for the undoped SnS and SnS:V 6% samples are presented in Figure 6. The intensity of the PL signal depends on the excitation intensity I_{ex} as:

$$I_{PL} = A * I_{ex}^{\gamma} \quad (1)$$

where A and γ are constants. The type of the observed transition is dependent on γ . A donor-acceptor transition is defined by $\gamma < 1$, a band-to-band transition by $\gamma = 1$, transitions involving excitons by $1 < \gamma < 2$ [25]. Fitting the PL data to Equation 1 gives $\gamma = 0.54 \pm 0.08$ for the undoped SnS samples and around $\gamma = 0.8$ for all the SnS:V samples (Table 2). The calculated γ values thus suggest the donor-acceptor transition. However, the peak energy fits the bandgap energy very well, which strongly points to band-to-band recombination.

The evolution of the PL spectrum with temperature is dependent on the type of transition. When the defects take part in the recombination processes, the PL will be quenched due to thermal emission from a defect level prevailing over the radiative recombination. The thermal activation energy of this shallower defect taking part in the recombination can then be calculated using [26]:

$$PL \propto \frac{1}{1 + T^{3/2} \sum_{i=1} a_i e^{-E_{ai}/k_B T}}, \quad (2)$$

where a_i is a constant that includes the capture cross-section, E_{ai} is the thermal activation energy of the defect, and k_B is the Boltzmann constant. The quenching of PL spectra for the undoped SnS and SnS:V 6% samples are presented in Figure 6a, with their resultant activation energies listed in Table 2.

PL due to band-to-band recombination does not depend on the temperature, except in the shifting of the PL peak to lower energies due to a bandgap change. Here the PL spectra depend weakly on temperature, and the activation energies of thermal quenching are low, being on the order of millielectronvolts. This means that there is a mechanism of non-radiative recombination being activated with temperature, which starts to prevail over the radiative recombination when the temperature increases. Low activation energies suggest that they are not related to a defect level but to some other mechanism. For example, this can be the activation over small barriers within the band arising from band fluctuations [27]. In such a case, the carriers move within the band, hopping over the potential fluctuations until they find a non-radiative recombination path. The recombination paths can be related to spatially localized defect clusters, dislocations, or grain boundaries. This mechanism is schematically presented in Figure 7 and has been previously observed, such as in SiC [28][29].

Conductivity

Apart from high absorption and good morphology, materials that absorb light in a solar cell should also be able to transport the photo-generated carriers to the external circuit without significant losses. Figure 8 presents the conductivity dependence on temperature for all the SnS thin films. The conductivity depends exponentially on T^{-1} with thermal activation energy E_a , which can be obtained from a linear fit to the logarithm of conductivity versus T^{-1} . The conductivity of the undoped SnS sample only follows this dependence above approximately 250 K, with $E_a = 379$ meV, whereas the conductivity is approximately constant at lower temperatures. The conductivity becomes thermally activated across the full range of temperatures in the V-doped samples. The activation energy is slightly lower, decreasing to 352 meV in the SnS:V 6% sample. The calculated activation energy can be in a p-type semiconductor, energy of a main acceptor but can also be related to any potential barrier i.e. located at the grain boundaries. The fact that the activation energy changes rather points into lowering a potential barrier at the grain boundaries assuming that the main acceptor responsible for conductivity in SnS is the same in all the samples. The conductivity of the samples increases, with a factor of 3.3 increase in conductivity between the undoped SnS and SnS:V 6% samples at 300 K. This increase can be related to the lowering of the activation energy, which then leads to an actual factor of 2.8 increase in conductivity after taking the reduced activation energy into account.

Conclusions

In this work we have presented a comparative study of the optical and electrical properties of vanadium-doped SnS thin films made by spray pyrolysis. XRD analysis revealed an orthorhombic structure of the investigated thin films, with (111) being the preferred crystallographic direction of crystallites. The films consist of a polycrystalline structure with longitudinal grains. V-doping slightly increases the crystallite size, but the average grain sizes are similar within the uncertainty range. The material has an indirect bandgap slightly below 1.1 eV. V-doping increases the absorption, but the absorption edge loses its clear direct character, and the absorption threshold increasing to around 1.2 eV. The PL study reveals a band-to-band dominant transition with an additional sharp peak in the V-doped samples, which we attribute to the transition between atomic orbitals in vanadium. Based on the PL results, we also suggest the existence of spatially localized defects taking part in non-radiative recombination. The conductivity increases in the V-doped SnS samples, which we attribute to the lowering of their activation energies.

Acknowledgements

This work was supported by the Minister den Economic y Competitividad (ENE2016-77798-C4-2-R) and Generalitat Valencia (Prometeus 2014/044).

References

- [1] W. Shockley, H.J. Queisser, Detailed balance limit of efficiency of p-n junction solar cells, *J. Appl. Phys.* 32 (1961) 510–519. doi:10.1063/1.1736034.
- [2] S. Rühle, Tabulated values of the Shockley-Queisser limit for single junction solar cells, *Sol. Energy.* 130 (2016) 139–147. doi:10.1016/j.solener.2016.02.015.
- [3] A. Luque, A. Martí, Increasing the Efficiency of Ideal Solar Cells by Photon Induced Transitions at Intermediate Levels, *Phys. Rev. Lett.* 78 (1997) 5014–5017. doi:10.1103/PhysRevLett.78.5014.
- [4] A. Luque, A. Martí, Fundamentals of Intermediate Band Solar Cells, in: A. Cristobal, M. Vega, L. Antonio, A. López (Eds.), *Next Gener. Photovoltaics New Concepts*, Vol. 165, Springer, 2012: pp. 209–228.
- [5] P. Palacios, I. Aguilera, K. Sánchez, J.C. Conesa, P. Wahnón, Transition-metal-substituted indium thiospinels as novel intermediate-band materials: Prediction and understanding of their electronic properties, *Phys. Rev. Lett.* 101 (2008) 2–5. doi:10.1103/PhysRevLett.101.046403.
- [6] P. Wahnón, C. Tablero, Ab initio electronic structure calculations for metallic intermediate band formation in photovoltaic materials, *Phys. Rev. B - Condens. Matter Mater. Phys.* 65 (2002) 1–10. doi:10.1103/PhysRevB.65.165115.
- [7] J.P. Mailoa, A.J. Akey, C.B. Simmons, D. Hutchinson, J. Mathews, J.T. Sullivan, D. Recht, M.T. Winkler, J.S. Williams, J.M. Warrender, P.D. Persans, M.J. Aziz, T. Buonassisi, Room-temperature sub-band gap optoelectronic response of hyperdoped silicon, *Nat. Commun.* 5 (2014) 1–8. doi:10.1038/ncomms4011.
- [8] K. Sánchez, I. Aguilera, P. Palacios, P. Wahnón, Assessment through first-principles calculations of an intermediate-band photovoltaic material based on Ti-implanted silicon: Interstitial versus substitutional origin, *Phys. Rev. B* 79 (2009) 165203. doi:10.1103/PhysRevB.79.165203.
- [9] P. Chen, M. Qin, H. Chen, C. Yang, Y. Wang, F. Huang, Cr incorporation in CuGaS₂ chalcopyrite: A new intermediate-band photovoltaic material with wide-spectrum solar absorption, *Phys. Status Solidi Appl. Mater. Sci.* 210 (2013) 1098–1102. doi:10.1002/pssa.201228721.
- [10] M.A. Flores, E. Menéndez-Proupin, W. Orellana, J.L. Peña, Sn-doped CdTe as promising intermediate-band photovoltaic material, *J. Phys. D. Appl. Phys.* 50 (2017). doi:10.1088/1361-6463/50/3/035501.
- [11] R. Lucena, I. Aguilera, P. Palacios, P. Wahnón, J.C. Conesa, Synthesis and Spectral Properties of Nanocrystalline V-Substituted In₂S₃, a Novel Material for More Efficient Use of Solar Radiation, *Chem. Mater.* 20 (2008) 5125–5127. doi:10.1021/cm801128b.

- [12] O.A. Yassin, A.A. Abdelaziz, A.Y. Jaber, Structural and optical characterization of V- and W-doped SnS thin films prepared by spray pyrolysis, *Mater. Sci. Semicond. Process.* 38 (2015) 81–86. doi:10.1016/j.mssp.2015.03.050.
- [13] J. Vidal, S. Lany, M. D’Avezac, A. Zunger, A. Zakutayev, J. Francis, J. Tate, Band-structure, optical properties, and defect physics of the photovoltaic semiconductor SnS, *Appl. Phys. Lett.* 100 (2012). doi:10.1063/1.3675880.
- [14] K. Santhosh Kumar, C. Manoharan, S. Dhanapandian, A. Gowri Manohari, T. Mahalingam, Effect of indium incorporation on properties of SnS thin films prepared by spray pyrolysis, *Optik (Stuttg.)* 125 (2014) 3996–4000. doi:10.1016/j.ijleo.2014.01.144.
- [15] S.H. Chaki, M.D. Chaudhary, M.P. Deshpande, Effect of indium and antimony doping in SnS single crystals, *Mater. Res. Bull.* 63 (2015) 173–180. doi:10.1016/j.materresbull.2014.12.013.
- [16] T.G. Hibbert, M.F. Mahon, K.C. Molloy, L.S. Price, I.P. Parkin, Deposition of tin sulfide thin films from novel, volatile (fluoroalkylthiolato)tin(IV) precursors, *J. Mater. Chem.* 11 (2001) 469–473. doi:10.1039/b005863g.
- [17] T. Sall, M. Mollar, B. Marí, Substrate influences on the properties of SnS thin films deposited by chemical spray pyrolysis technique for photovoltaic applications, *J. Mater. Sci.* 51 (2016) 7607–7613. doi:10.1007/s10853-016-0039-9.
- [18] T. Sall, M. Mollar, B. Marí, Tin-mono-sulfide (SnS) thin films prepared by chemical spray pyrolysis with different [S]/[Sn] ratios, *Opt. Quantum Electron.* 49 (2017). doi:10.1007/s11082-017-1219-9.
- [19] T.H. Sajeesh, A.R. Warriar, C.S. Kartha, K.P. Vijayakumar, Optimization of parameters of chemical spray pyrolysis technique to get n and p-type layers of SnS, *Thin Solid Films.* 518 (2010) 4370–4374. doi:10.1016/j.tsf.2010.01.040.
- [20] R. Sivaramasubramaniam, R. Muhamad, S. Radhakrishna, Optical Properties of Annealed Tin(II) Oxide in Different Ambients, *Phys. Status Solidi.* 136 (2006) 215–222. doi:10.1002/pssa.2211360126.
- [21] M. Parenteau, C. Carlone, Influence of temperature and pressure on the electronic transitions in SnS and SnSe semiconductors, *Phys. Rev. B.* 41 (1990) 5227–5234. doi:10.1103/PhysRevB.41.5227.
- [22] H. Kato, N. Kashio, Y. Ohki, K.S. Seol, T. Noma, Band-tail photoluminescence in hydrogenated amorphous silicon oxynitride and silicon nitride films, *J. Appl. Phys.* 93 (2003) 239–244. doi:10.1063/1.1529292.
- [23] J. Heikenfeld, M. Garter, D.S. Lee, R. Birkhahn, A.J. Steckl, Red light emission by photoluminescence and electroluminescence from Eu-doped GaN, *Appl. Phys. Lett.* 75 (1999) 1189–1191. doi:10.1063/1.124686.
- [24] F. Briones, D.M. Collins, Low temperature photoluminescence of lightly Si-doped and undoped MBE GaAs, *J. Electron. Mater.* 11 (1982) 847–866. doi:10.1007/BF02672399.

- [25] J.I. Pankove, Radiative Transitions, in: Opt. Process. Semicond., Dover Publications, Inc., New York, 1971.
- [26] H. Shibata, Negative thermal quenching curves in photoluminescence of solids, Japanese J. Appl. Physics, Part 1 Regul. Pap. Short Notes Rev. Pap. 37 (1998) 550–553. doi:10.1017/CBO9781107415324.004.
- [27] J.P. Leitão, N.M. Santos, P.A. Fernandes, P.M.P. Salomé, A.F. Da Cunha, J.C. González, G.M. Ribeiro, F.M. Matinaga, Photoluminescence and electrical study of fluctuating potentials in Cu₂ZnSnS₄-based thin films, Phys. Rev. B - Condens. Matter Mater. Phys. 84 (2011) 1–8. doi:10.1103/PhysRevB.84.024120.
- [28] J. Robertson, Recombination and photoluminescence mechanism in hydrogenated amorphous carbon, Phys. Rev. B - Condens. Matter Mater. Phys. 53 (1996) 16302–16305. doi:10.1103/PhysRevB.53.16302.
- [29] G.S. Fu, X.Z. Wang, W.B. Lu, W.L. Dai, X.K. Li, W. Yu, Structural and band tail state photoluminescence properties of amorphous SiC films with different amounts of carbon, Chinese Phys. B. 21 (2012). doi:10.1088/1674-1056/21/10/107802.

Table 1. XRD (crystallite) and AFM (grain) data for the SnS films.

sample	crystallite size [nm]	mean grain size [nm]	mean roughness height [nm]
Undoped SnS	19.0 ± 0.4	32.7 ± 4.9	32.8 ± 3.2
SnS:V 2%	18.5 ± 0.4	45.0 ± 7.1	41.2 ± 4.1
SnS:V 4%	19.4 ± 0.4	33.0 ± 6.6	35.5 ± 6.1
SnS:V 6%	20.4 ± 0.5	37.0 ± 5.3	36.2 ± 5.3

Table 2. Photoluminescence (PL) spectra parameters for the undoped and V-doped SnS films.

sample	[a.u.]	[eV]	[meV]
Undoped SnS	0.56 ± 0.08	0.17 ± 0.02	5.7 ± 0.9
SnS:V 2%	0.80 ± 0.06	0.23 ± 0.03	4.2 ± 0.2

SnS:V 4%	0.78 ± 0.02	0.21 ± 0.04	4.6 ± 0.4
SnS:V 6%	0.80 ± 0.02	0.26 ± 0.04	4.5 ± 0.3

Figure 1. A schematic diagram of the possible optical transitions in a semiconductor having a bandgap energy E_g and an intermediate band (IB) located within the forbidden energy gap. This creates the availability of two optical transitions, with energies $E_g/2 < E_1 < E_g$ and $E_2 < E_g/2$.

Figure 2. XRD spectra of the V-doped SnS thin films. The results for of the SnS thin films doped with 0%, 2%, 4%, and 6% vanadium in the sprayed solution are shown, and the preferential crystallographic directions are identified.

Figure 3. AFM images of an undoped SnS thin film (left image) and an SnS thin film doped with 6% vanadium in the sprayed solution (right image).

Figure 4. (a) Absorption coefficient and (b) transmission for the films for different degrees of V-doping. For calculation of absorption coefficient thickness of $0.4 \mu\text{m}$ was taken. The inset in (a) includes the $(\alpha h\nu)^{-2}$ fits to the undoped SnS and SnS:V 6% samples, shown as black lines, which yield the bandgap energy.

Figure 5. Photoluminescence (PL) spectra for the SnS:V thin films. The red line on the undoped SnS PL spectrum provides an example of fitting the low-energy slope of the PL peak with the exponential function.

Figure 6. Integrated area of the PL spectra measured at 9.6 K as a function of (a) laser power and (b) temperature. The best-fit curves to the data in (a) and (b) are from Equations 1 and 2, respectively.

Figure 7. Schematic band diagram for the proposed mechanism of PL quenching of the band-to-band recombination. Luminescence occurs by recombination of the electron-hole pairs in the bulk material. Non-radiative recombination lowers the PL signal and takes place after the hopping of charge carriers through the potential fluctuation to a spatially localized defect.

Figure 8. Temperature dependence of electrical conductivity for the investigated thin films. Linear fits were made in the 250–330 K range for each of the samples.

ACCEPTED MANUSCRIPT

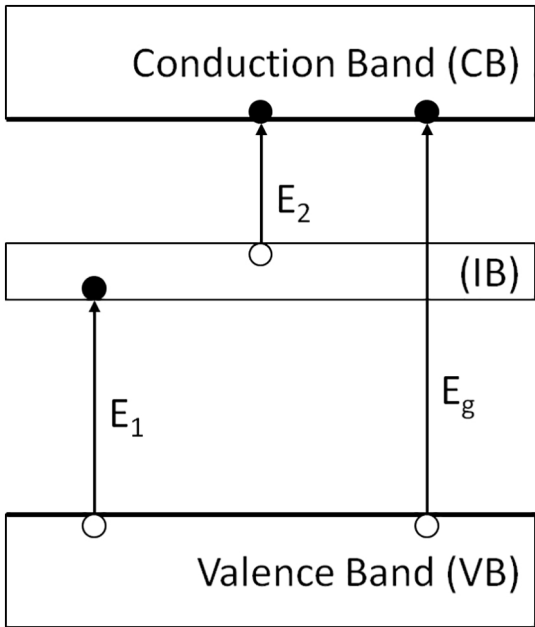


Figure 1

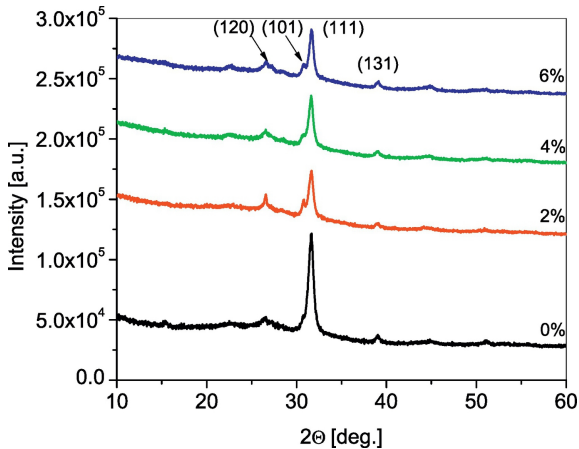


Figure 2

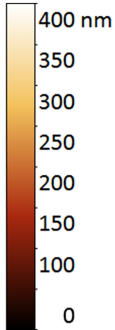
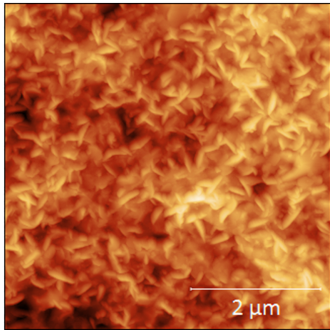
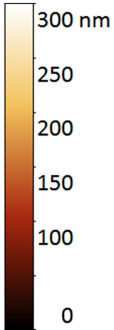
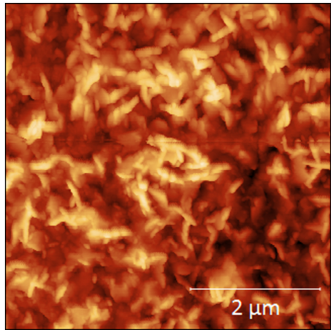


Figure 3

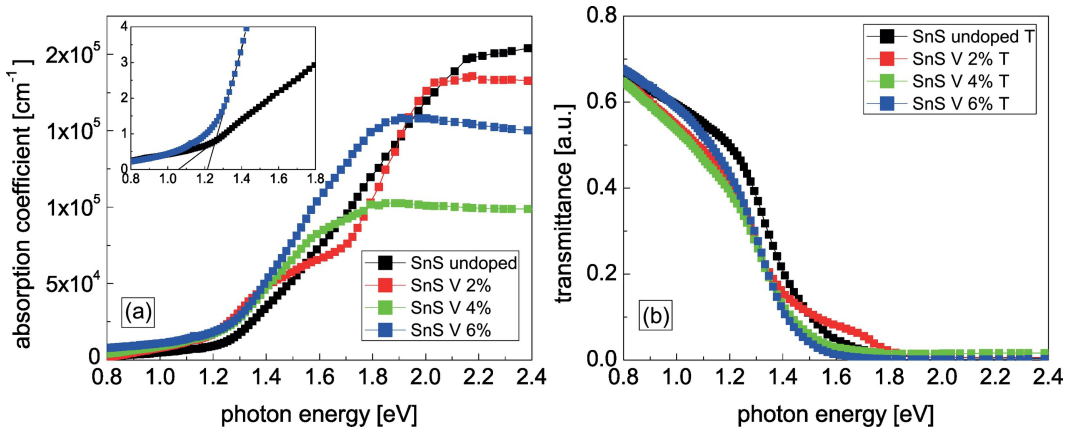


Figure 4

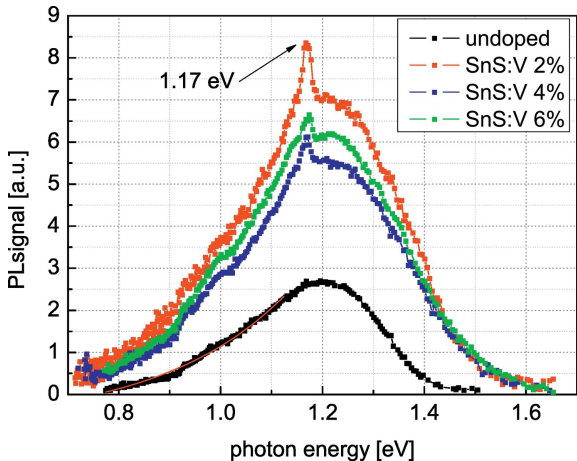


Figure 5

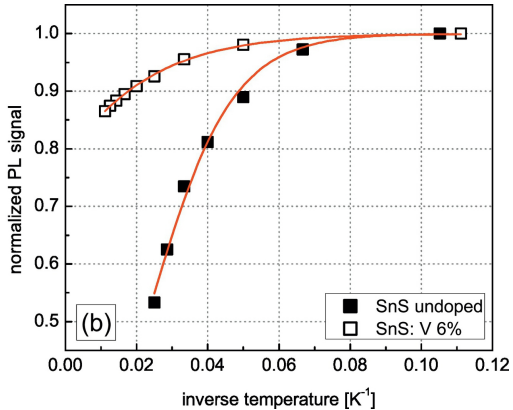
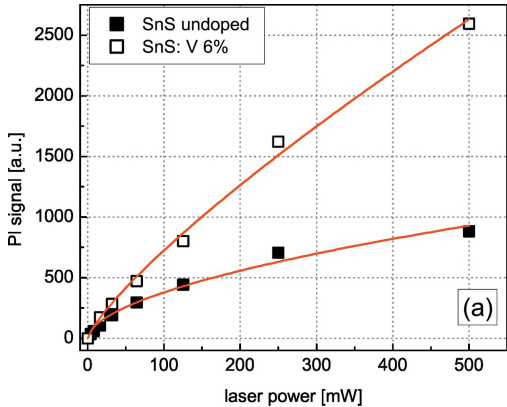


Figure 6

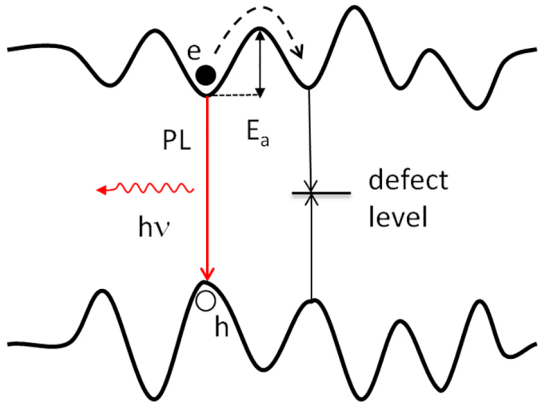


Figure 7

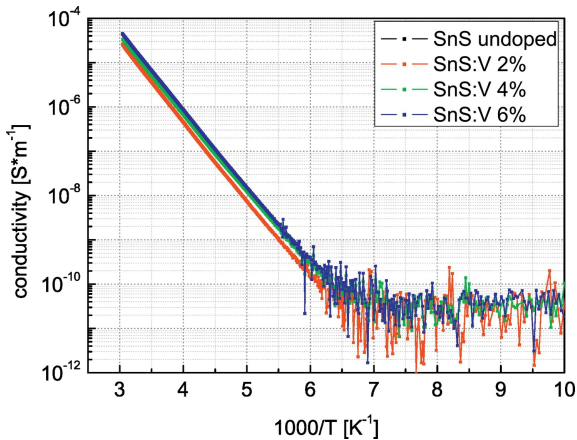


Figure 8